Development of a Photothermal Treatment Planning Workflow for use in Synergistic Immuno-Photothermal-Nanotherapy (SYMPHONY)

by

Mason Scott Hazlett

Graduate Program in Medical Physics
Duke University

Date: _____

Approved:

_____
Gregory Palmer, Supervisor

_____
Mark Dewhirst

_____
Brant Inman

Thesis submitted in partial fulfillment of
the requirements for the degree of
Master of Science in the Graduate Program in
Medical Physics in the Graduate School
of Duke University

2022

ABSTRACT

Development of a Photothermal Treatment Planning Workflow for use in Synergistic Immuno-Photothermal-Nanotherapy (SYMPHONY)

by

Mason Scott Hazlett

Graduate Program in Medical Physics
Duke University

Date: _____
Approved:

_____
Gregory Palmer, Supervisor

_____
Mark Dewhirst

_____
Brant Inman

An abstract of a thesis submitted in partial fulfillment of
the requirements for the degree
of Master of Science in the Graduate Program in
Medical Physics in the Graduate School
of Duke University

2022

Abstract

Approximately half of bladder cancer diagnoses are late stage/show metastatic spread. The current standard treatment option for these diagnoses is cisplatin chemotherapy, however 40% of patients are ineligible to receive this treatment, leaving few alternatives. The most common alternative to chemotherapy that is currently used is immune checkpoint blockade or immunotherapy. However, immunotherapy alone has proven largely ineffective as a curative treatment option for the metastatic disease, indicating a critical need for new systemic treatment options.

Our group has previously demonstrated in a pilot study the efficacy of a novel combination therapy incorporating two treatment arms: clinically available immunotherapy and gold nanostar mediated photothermal therapy (abbreviated as PTT). This treatment is called Synergistic Immuno Photothermal Nanotherapy (abbreviated as SYMPHONY). In this study, C57BL/6 mice were implanted with MB49 bladder cancer cells at two locations. One of the two subsequent tumors was treated with one of five total treatment arms. After treatment, one of the mice treated with SYMPHONY showed total tumor local control and no tumor regrowth upon MB49 cell rechallenge, suggesting long term cancer immunity induced by SYMPHONY treatment.

Currently, the treatment paradigm for SYMPHONY follows as: 1) Gold nanostar (abbreviated as GNS) injection followed by a 24-hour waiting period 2) Mice are put

under anesthesia and laser irradiation of the tumor is performed at a constant power density for 10 minutes 3) Anti-PD-L1 immunotherapy injections are given following irradiation. For SYMPHONY's photothermal therapy treatment arm, quantitative characterization of the GNS photothermal effect and a photothermal treatment planning process are crucial aspects of SYMPHONY that **remain undeveloped.**

The **overall goal** of SYMPHONY is to provide a systemic, curative treatment option for patients diagnosed with late-stage bladder cancer. The **objective** of this work is to characterize the photothermal effect as well as develop and validate a photothermal treatment planning workflow to be used in SYMPHONY treatment that accurately predicts thermal dose delivery. The goals of this work were completed using a variety of **materials and methods**, including: In vitro agarose-GNS gel phantoms along with thermocouples for thermal dosimetry, radiative transport and heat transfer software used to create photothermal simulations, a multitude of characterization methods to extract key GNS physical properties, as well as image segmentation and model generation techniques to analyze animal images and create simulation models.

Results from *in vitro* phantom heating studies and their accompanying photothermal simulations are presented. Additionally, optical absorption characterization data is presented to serve as the basis for selected optical modeling parameters. Trends in GNS-mediated photothermal effect and the dependence on

concentration are discussed, as well as their implications for future SYMPHONY studies.

Contents

List of Figures

1. Introduction

1.1 Bladder Cancer

Development of bladder cancer (BC) generally begins in the transitional epithelium (inner lining) cells of the bladder. As the disease progresses, it can invade deeper layers of the bladder, including muscle and surrounding fatty tissues. Due to this spread, there is an increased likelihood of metastasis or lymph node involvement and thus, a reduced number of viable, curative treatment options. Early-stage diagnoses of bladder cancer fortunately have higher five-year survival rates, however these diagnoses only account for 50% of all diagnoses (generally due to lack of public screening), while the remaining are advanced and potentially involve a form of metastasis or lymphatic spread [1,2]. In these advanced cases, standard treatment options become ineffective, indicating a dire need for the development of new systemic and translational therapies.

1.2 Treatment Options for Bladder Cancer

The current standard and primary treatment option for non-muscle invasive bladder cancer is direct surgical resection of the visible disease, with additional margins for surrounding tissue. Adjuvant chemotherapy can also be considered, however these options often lead to lowered quality of life and accompanying chemotherapy side effects. Importantly, these options can be ineffective when treating metastatic bladder cancer, as direct resection does not treat the metastatic disease, requiring additional chemotherapy.

For patients with an advanced diagnosis, the primary treatment option is cisplatin-based chemotherapy, which has proven effective at inducing complete response and high long-term survival rates [3]. However, between 30-40% of patients do not qualify for this treatment. If a patient does not qualify for cisplatin chemotherapy, few viable treatment options remain.

Current research and early implementations of immunotherapy and combination therapies offer promising alternative treatment options for patients ineligible for chemotherapy and provide a potential solution to the clinical needs present when treating bladder cancer.

1.3 Immunotherapy for the Treatment of Bladder Cancer

Immunotherapies (also referred to immune checkpoint inhibition) used for the treatment of bladder cancer have completely revolutionized the landscape of curative treatment options. PD1 and PD-L1 immune checkpoint inhibiters have shown great promise as an alternative treatment for patients that are cisplatin ineligible [4].

One such immunotherapy, which has shown strong success rates (three-year disease-free survival and progression-free survival of 66.2% and 86.8%, respectively) in responding patients with non-muscle-invasive bladder cancer, is bacillus Calmette-Guérin (BCG) [5]. However, BCG is ineffective when treating patients with muscle-invasive BC, as only the superficial tumor is treated by the induced immune response. One reason for this outcome, as is common across multiple cancer types, is the

expression of programmed death-ligand (PD-L1) on cancer cells that disables the inherit anti-cancer immune response of programmed cell-death 1 (PD-1) expression on immune cells [6].

Briefly summarized, PD-1 is an inhibitory receptor on the surface of T-cells that suppresses T-cell activation by binding to ligands PD-L1 and PD-L2 and transmitting inhibiting signals (immune "checkpoints"). This process regulates natural immune response to prevent destruction of healthy cells. Cancer cells often overexpress PD-L1 relative to T-cell PD-1 expression, allowing the cancer to evade natural immune response altogether. The PD-1/PD-L1 interaction can be inhibited using antibodies (the basis for anti-PD-L1/PD-1 immunotherapy) that block the binding interaction, recovering the anti-cancer immune response [7].

Currently, there are clinically available immunotherapies that have been employed for the treatment of muscle-invasive bladder cancer, however only up to 40% of patients can potentially be cured with this therapy, indicating that immunotherapy alone is not a curative treatment alternative for cisplatin-ineligible BC patients [8]. Our group aims to provide a curative and systemic alternative treatment option for muscle-invasive BC by synergizing the effects of anit-PD-L1 immunotherapy with photothermal therapy.

1.4 Hyperthermia and Gold Nanoparticle-Mediated Photothermal Therapy for the Treatment of Bladder Cancer

Hyperthermia has been used in cancer treatment for decades and has proven to be a powerful primer that improves local control rates when combined with standard treatments like chemotherapy and radiation therapy. Generally, there are two types of hyperthermia: mild-moderate (38 – 43 degrees Celsius) and high (above 44 degrees Celsius), both of which are externally induced, typically by laser source. High temperature hyperthermia directly induces cell death to both malignant and healthy cells. When heated in the mild-moderate range, many positive effects are observed that promote an anti-cancer response, including tumor reoxygenation, vascular perfusion, enhanced immune cell infiltration and function, as well as radio sensitization [9]. In the context of plasmonic photothermal therapy (PTT) mediated by gold nanoparticles, incident radiation at a wavelength like the periphery of the nanoparticle (surface plasmon resonance effect) is converted to tissue heating, shown in Figure 1 [10].

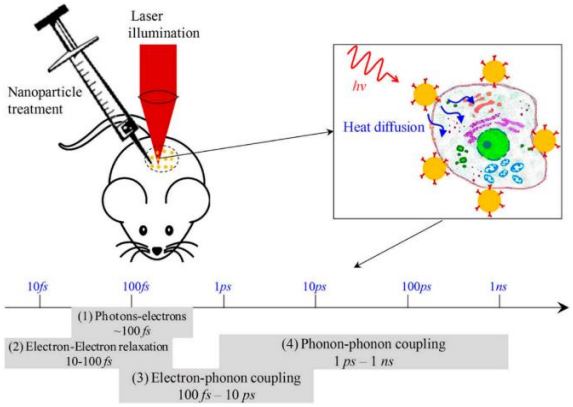

Figure 1: Illustrative Physical Process for PTT mediated by gold nanoparticles.

Tunability of certain properties of these nanoparticles, including shape, composition, size, and resonance wavelength contribute to the utility of a given nanoparticle. For this work, gold nanostars (GNS) are used for their highly optimal photothermal conversion efficiency (tunable plasmon resonance to incident light) and "lightning rod" effect due to the star branches acting as hotter locations for heat delivery [11].

Additionally, due to the size and shape of the GNS, they have an enhanced permeability and retention effect (EPR), which is defined as the ability of the nanoparticle to preferentially accumulate in the tumor. Enhanced cell membrane permeability during heating as well as inherently reduced tumor lymphatic drainage contribute to the EPR effect and are essential in maximizing tumor delivery of GNS [12]. The above characteristics of nanoparticles and hyperthermia are vital to consider when developing a plasmonic photothermal therapy platform, which will be outlined next.

1.5 Synergistic Immuno-Photothermal-Nanotherapy (SYMPHONY)

Synergistic Immuno-Photothermal-Nanotherapy (referred to as SYMPHONY) is a novel combination therapy designed to be a viable, curative treatment option for patients with metastatic bladder cancer that are cisplatin-ineligible. SYMPHONY combines two treatment arms, anti-PD-L1 immunotherapy and gold nanostar mediated photothermal ablation, to achieve both direct primary tumor cell killing and systemic immune response (abscopal effect).

A previously published mice pilot study for SYMPHONY demonstrated complete primary and distant tumor eradication, as well as resulted in higher local control and survival rates than any of the other individual treatment or combination of treatments. Additionally, mice treated with SYMPHONY were rechallenged with cancer cells and showed complete resistance to tumor regrowth, indicating a long term, systemic anti-cancer immunity induced by SYMPHONY treatment [13].

In preparing SYMPHONY for translation into human trials, continued developments in both treatment arms (with the photothermal therapy arm being the focus of this work) are required and will be outlined in subsequent sections.

2. Materials and Methods

2.1 Gold Nanostar Synthesis

Synthesis of GNS used in this work was performed following the method outlined in [11]. Briefly summarized here, gold sphere nanoparticles were synthesized by reducing $HAuCl_4$ with trisodium citrate and then used as seeds, quickly mixed with $AgNO_3$, ascorbic acid and $HAuCl_4$. Synthesized GNS were then coated with polyethylene glycol by gold-thiol bond.

2.2 Material Characterization of Gold Nanostars

To translate a new nanotechnology into standard clinical use, careful investigation of many properties of the technology must be performed to determine the safety and efficacy of its use. Cytotoxicity, biocompatibility and biodistribution are some key aspects of nanotechnology that must be validated before standard use (in particular, receiving FDA approval).

As summarized above, gold nanoparticles have been shown to have good biocompatibility and tunable biodistribution/tumor uptake (through targeted functionalization techniques) and are performing well in completed and on-going clinical trials. In the context of SYMPHONY treatment, similar characterization of GNS will be a vital component for clinical translation. SYMPHONY's members have performed studies investigating GNS tumor uptake/biodistribution previously [14].

However, complete optical, thermal, and dielectric characterization of GNS remains uninvestigated.

Determination of these properties across a range of biologically relevant GNS concentrations will forward SYMPHONY treatment in two ways; firstly, in the ability to present accurate physical properties of the GNS when pursuing FDA approval and secondly (especially important for this work) is incorporating the values of these properties into photothermal simulations to improve the accuracy of SYMPHONY predictive treatment planning (detailed in Section 2.5).

2.2.1 Optical Absorption

Gold nanostars derive their clinical appeal from their NIR absorption enhancing properties (surface plasmon resonance) and high photothermal conversion efficiency. Accurate characterization of their optical absorption spectra both as a function of wavelength and as a function of concentration for a given wavelength will be crucial to demonstrating therapeutic control of the GNS. Additionally, the optical absorption coefficient is a key parameter used in this work to develop the photothermal simulation method (outlined in subsequent sections).

A standard method used in optical and size characterization of gold nanoparticles is UV-VIS Spectroscopy [15]. In this work, a uniformly mixed sample of agarose gel and 0.5 nM GNS was placed in a cuvette (pathlength of 1 cm) for analysis in

a UV-VIS Spectrophotometer. Absorbance data was collected for wavelengths between 200 and 1400 nm.

The relationship between absorption and concentration is determined by the Beer-Lambert Absorption Law, given by Equation 1 below [16]. Using the result of the 0.5 nM optical absorbance spectra and, the absorbance as a function of GNS concentration can be plotted and subsequently used in photothermal modeling.

$$A = \epsilon b c$$

2.3 Monte Carlo and Finite Element Predictive Modeling

Treatment planning, across multiple types of radiation therapy, is a crucial and often necessary component for clinical implementation and standardization of a radiation treatment. Development of a photothermal simulation workflow that accurately predicts thermal dose delivery during SYMPHONY's PTT treatment is vital for future translation of SYMPHONY into human trials.

For this work, the photothermal effect mediated by GNS is characterized *in vitro* using thermal dosimetry methods. These experiments and the resulting temperature data are accompanied by photothermal simulations for validation of the simulation workflow. These simulations are created using a combination of Monte Carlo and finite element strategies, summarized below.

2.3.1 Radiative Transport and Heat Transfer

The physics underlying SYMPHONY's PTT arm can be divided into two kinds: Radiative Transport and Heat Transfer. The transport component, in the context of SYMPHONY treatment, describes the interaction between incident photons from the treatment laser and biological tissue. This process can be considered the "photo" portion of photothermal therapy. Incoming photons interact with the tissue, absorbing and scattering as they propagate. The inclusion of GNS in the tumor amplifies the optical photon absorption relative to the tissue by itself, leading to increased energy deposition. The resulting enhanced energy absorption in the tissue acts as a heat source, which is then described using a heat transfer process; the "thermal" in photothermal therapy. The local heating produced during these interactions represents the therapeutic strategy of SYMPHONY; that is, to raise and maintain the tumor temperature to the mild hyperthermia range (43 degrees Celsius) and above to induce both direct cell-killing and systemic, immunologic responses.

The combination of these physical processes is described through a set of two coupled differential equations, summarized below. A major focus of this work, in the context of developing a treatment planning simulation workflow, was to identify techniques (both computational and experimental) that correctly simulate the results of these differential equations and their parameters. Successful implementation of these

techniques will lead to an accurate treatment planning method that can be incorporated into the SYMPHONY treatment workflow.

The Radiative Transport Equation (RTE) governs the interaction of photons with biological tissue and is given by Equation 2 below. This equation describes the transfer of energy to the tissue as the incident photons pass through.

$$\frac{\partial \mathrm{L}(\vec{r},\hat{s},t)/c}{\partial \mathrm{t}} + \hat{s}\cdot\nabla L(\vec{r},\hat{s},t) + \mu_t \mathrm{L}(\vec{r},\hat{s},t) = \mu_s \int_{4\pi} L\left(\vec{r},\widehat{s'},t\right) P(\widehat{s'},\hat{s}) d\Omega' + S(\vec{r},\hat{s},t)$$

The key optical parameters that define this process are the absorption coefficient μ_a, scattering coefficient μ_s , extinction coefficient μ_t (sum of absorption and scattering), scattering anisotropy g, and the source term $S(\vec{r},\hat{s},t)$. The solution to this equation is the radiance $L(\vec{r},\hat{s},t)$, which is an angular quantity describing the local area energy absorption per unit time per unit solid angle. μ_a is a measure of how much the incident radiation is absorbed after interacting with the tissue. The scattering coefficient is a measure of how the radiation scatters after interacting with tissue. Scattering anisotropy measures how much "forwardness" a photon retains after a scattering event and can be calculated by Equation 3 below.

$$g = \int_{4\pi} (\widehat{s'} \cdot \hat{s})\, P(\widehat{s'} \cdot \hat{s}) d\Omega$$

Anisotropy, in general, is between 0.9 and 0.95 for biological tissues, i.e., photons remain approximately forward scattered after initial interactions with tissue. The source term is the intensity distribution of the incident radiation and can dramatically alter the resulting radiance depending on the form it takes. After the photon source and optical properties are specified, the equation can be solved for the radiance. The local volumetric energy absorption is then calculated by integrating the radiance across the solid angle and multiplying by the absorption coefficient, shown in Equation 4 below.

$$\Phi(r,t) = \mu_a \int_{4\pi} L(r,\Omega) d\Omega$$

These values then serve as the input heat source to the heat transfer equation, leading to temperature increase over time. The relevant form of the heat transfer equation depends largely on the involved materials in the system (fluids, solids, metals, tissue, etc.) and can include varying terms to correctly model a given process.

In the context of SYMPHONY PTT, the Bioheat Transfer equation describes temperature evolution within biological tissues and is given by Equation 5 below.

$$\rho C_b \frac{dT}{dt} - \nabla \cdot (k\nabla T) = Q_{perf} + Q_e + Q_{met}$$

Here, Q_e is the calculated volumetric energy absorption resulting from (3). Q_{perf} is a source term that accounts for blood perfusion within the tissue and Q_{met} is a source term that accounts for metabolic activity. The solution to (5) gives a spatial and temporal temperature distribution within the solved geometry.

Given the heterogeneous nature of tumors and the above physical process for photothermal delivery, it is crucial that accurate optical and thermal properties be used when creating simulations that predict photothermal dose delivery during SYMPHONY treatment. This becomes particularly important since the tumors have been implanted with the GNS that function as optical absorption enhancers. Citing published literature as well as performing physical characterization experiments to determine the optical and thermal properties (described in Section 2.4) that accurately reflect the effects of GNS implanted in the tumor tissue will contribute to developing an accurate simulation model for treatment planning.

2.3.2 MCMatlab (Monte Carlo)

The gold standard to solving the RTE given in (2) is the Monte Carlo method which, computationally, has developed considerably over the last few decades,

famously with Monte Carlo for Multi-Layered Media (MCML) and subsequent improvements and adaptations [17]. RTE simulation work presented here is done using MCMatlab, a user friendly and Matlab-integrated RTE solver.

Briefly summarized, photon transport is simulated in a discretized or "voxelized" geometry, where each voxel is assigned optical properties (described in Section 2.5.1) by the user. A photon source is defined, and photon packets are launched governed by semi-random initial positions and trajectories. As the photons travel through the geometry, for a given voxel the photons deposit some of their energy, which is determined by the absorption coefficient of the voxel. Subsequent scattering occurs, determined by the scattering coefficient and anisotropy g of the voxel. The local energy absorption in each voxel within the geometry is iteratively stored after each simulated photon, resulting in a 3D matrix of volumetric energy absorption values once the simulation is complete [18].

Limited only by computational speed and desired simulation time, for a sufficiently large number of simulated photons, the simulation converges to the exact solution of the RTE. As described previously, for a correctly defined optical system (see MCMatlab blood vessel example in Figure 2), the solution to the Monte Carlo simulation will then serve as the input heat source to the Bioheat Transfer Equation to simulate SYMPHONY thermal dose delivery to the tumor implanted with GNS.

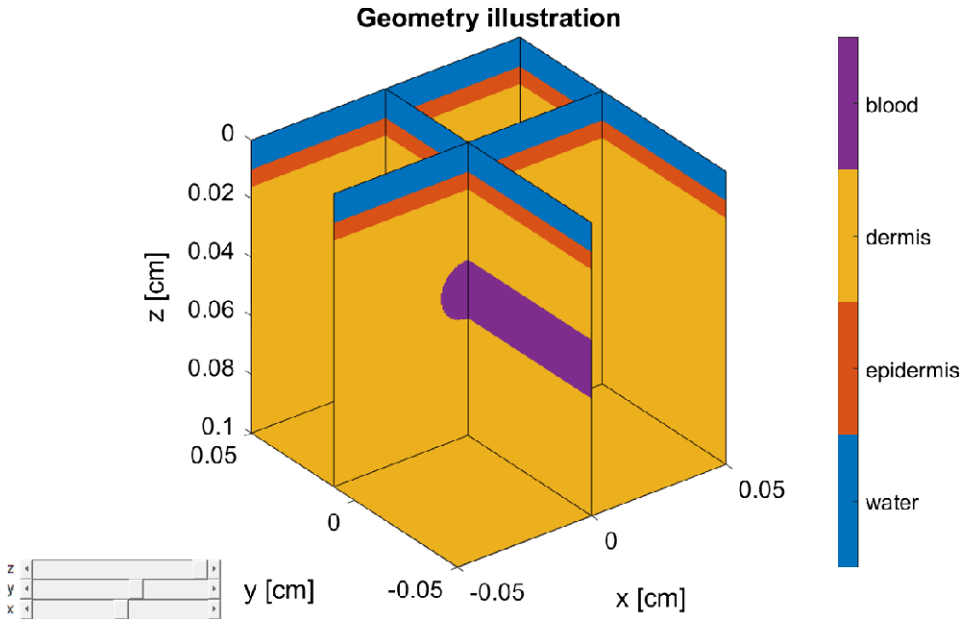

Figure 2: MCMatlab Example Blood Vessel Optical Geometry

In this work, the resulting 3D absorption matrix is then read into an output text file, with columns following the format (*x*, *y*, z, E), where *x*, *y* and *z* are the Cartesian coordinates of the simulated voxels and E is the volume energy absorption of each respective voxel. This output text file is then read into heat transfer software as a heat source.

2.3.3 COMSOL Multiphysics (Finite Element)

COMSOL Multiphysics ® is a commercial finite element simulation software that allows physics-based interfaces and coupled partial differential equations. For this work, the Heat Transfer and Bioheat Transfer modules were utilized to simulate the heating due to the volumetric energy absorption values calculated previously (see Section 2.3.2).

This software was used to simulate the *in vitro* laser heating experiments for validation of the proposed simulation method.

The finite element method has become a widely used technique for analysis of complex engineering and physics problems. Briefly summarized, this method discretizes an otherwise unsolvable system into a series of smaller subsystems to be solved individually. This is done by converting the geometry to be solved into a "mesh," which is comprised of smaller geometric "elements" where the problem is solved locally. Then, to approximate the total solution to the entire geometry (which would otherwise be impossible to solve numerically), a superposition of the local element solutions is performed. Simulation accuracy is determined by element shape and size, with smaller element size requiring higher computational power.

2.4 In Vitro Photothermal Characterization

Within the field of laser applications to cancer treatment, tissue mimicking optical phantoms are a powerful tool in characterizing thermal effects due to laser interactions in tissue. Phantom characterizations are often a crucial intermediate step in validating a laser therapy for translation into a clinical setting.

For SYMPHONY, tissue mimicking phantoms that incorporate a biologically relevant range of GNS concentrations are necessary for direct characterization of the photothermal effect mediated by the GNS. Performing phantom laser heating experiments to quantitatively characterize temperature rise during laser delivery, as

well as performing the subsequent heat transfer simulations will motivate the application of the proposed treatment planning workflow in animal studies.

In this work, both homogeneous and heterogeneous phantom laser heating experiments were performed, across the GNS range of 0–5 nM concentrations (informed by previous biodistribution studies). Thermal dosimetry was used to determine the temperature over time during laser delivery. Phantom fabrication and experimental setup are described in the following sections.

2.4.1 Homogenous Calibration Phantoms

Previous biodistribution studies performed in the SYMPHONY group informed the choice of GNS concentrations for photothermal characterization in phantoms. The range is given as 0 (blank), 0.01, 0.05, 0.1, 0.25, 0.5, 1, 2.5, 5 nanomolar (nM), with the nominal or "typical" GNS concentration being 0.5 nM (see figure at the end of Section 2.4.2)

Phantoms were created by uniformly mixing 3% (3 mg agarose powder to 100 mL of water) agarose gel and the corresponding GNS concentration, then pouring the mixture into two separate 3D printed cubic molds, one for the main body of the phantom and one for a thin, 2 mm layer on the top of the phantom mimicking surface skin tissue. The dimensions of the phantoms are 1.8 cm x 1.8 cm x 1.4 cm and are designed to be a closer approximation to tumors that are treated during SYMPHONY animal studies.

These homogeneous phantoms provide a simple and predictable geometric baseline (in particular, an approximately homogeneous optical system) that can be used for straightforward photothermal characterization and modeling.

2.4.2 Heterogenous Tumor-GNS Inclusion Phantoms

The heterogeneous phantoms were created in a similar way to the above homogeneous phantoms, but instead used 3D cubic molds that included a spherical inclusion at the center of the phantom to simulate a spherical tumor below the surface skin. In this case, GNS are only present within the internal spherical volume of radius 0.35 cm, while the rest of the surrounding phantom material is just the agarose gel, mimicking a tumor surrounded by normal tissue with no GNS uptake.

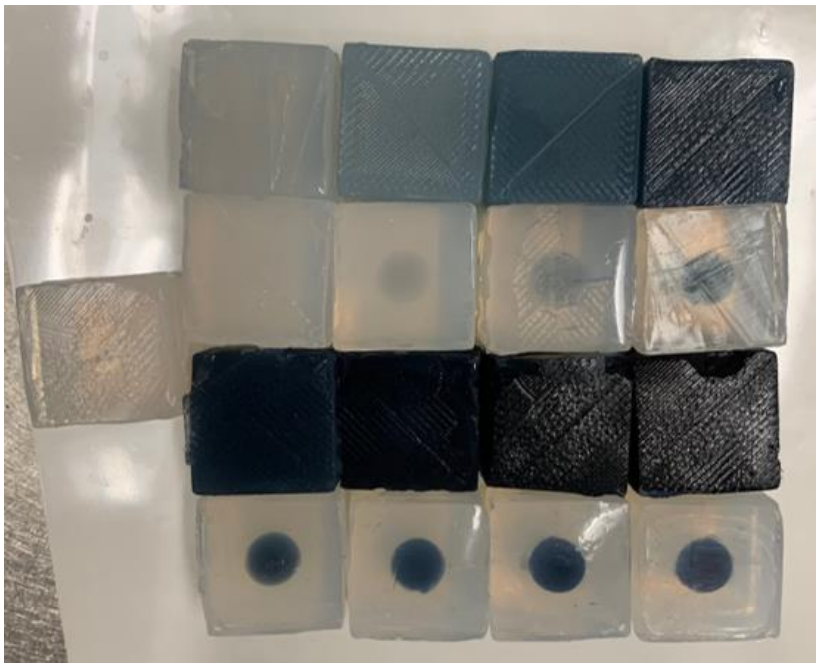

Figure 3: GNS phantoms used for laser delivery experiments. In order from top to bottom: 1st and 3rd rows are homogeneous phantoms, 2nd and 4th rows are heterogeneous phantoms (Photo Credit: Aidan Canning)

2.4.3 Experimental Design and Setup

The experimental design and setup chosen for this work includes two forms of laser delivery, physical staging of the phantom, a water circulation system, and thermal dosimetry. A 3D printed cylindrical stand was produced (see figure below) to stage the phantoms and hold a volume of water. Below the central phantom stage in the middle of the cylinder is an opening where a stir bar is housed. The entire cylinder is placed on top of a stir plate and the stir rod slowly circulates the water, maintaining a uniform temperature distribution in the cylinder.

A heat bath and water circulation system was created to maintain the water temperature at 37 degrees Celsius. This mimics the normal body temperature of mice before laser treatment. Heated water from the heat bath is circulated into the cylinder stage by plastic tubing, then removed and put back into the heat bath by a second array of tubing. Flow rates were fine-tuned until the water temperature remained at approximately 37 degrees Celsius, confirmed by thermocouple placed in the cylinder water.

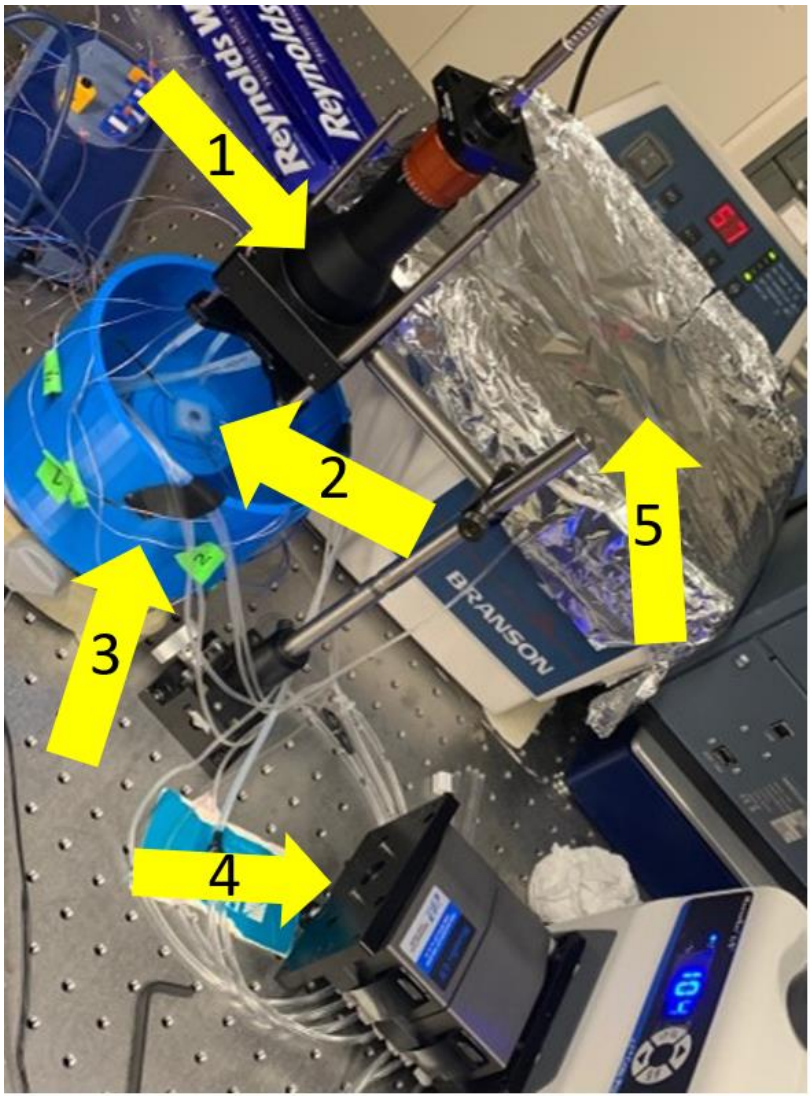

Figure 4: Experimental setup for phantom laser delivery. Arrow 1 is the collimated laser beam. 2 is the staged phantom with implanted thermocouples. 3 is the cylindrical stage placed on top of a stir board. 4 is the water circulation system and 5 is the heat bath. (Photo Credit: Aidan Canning)

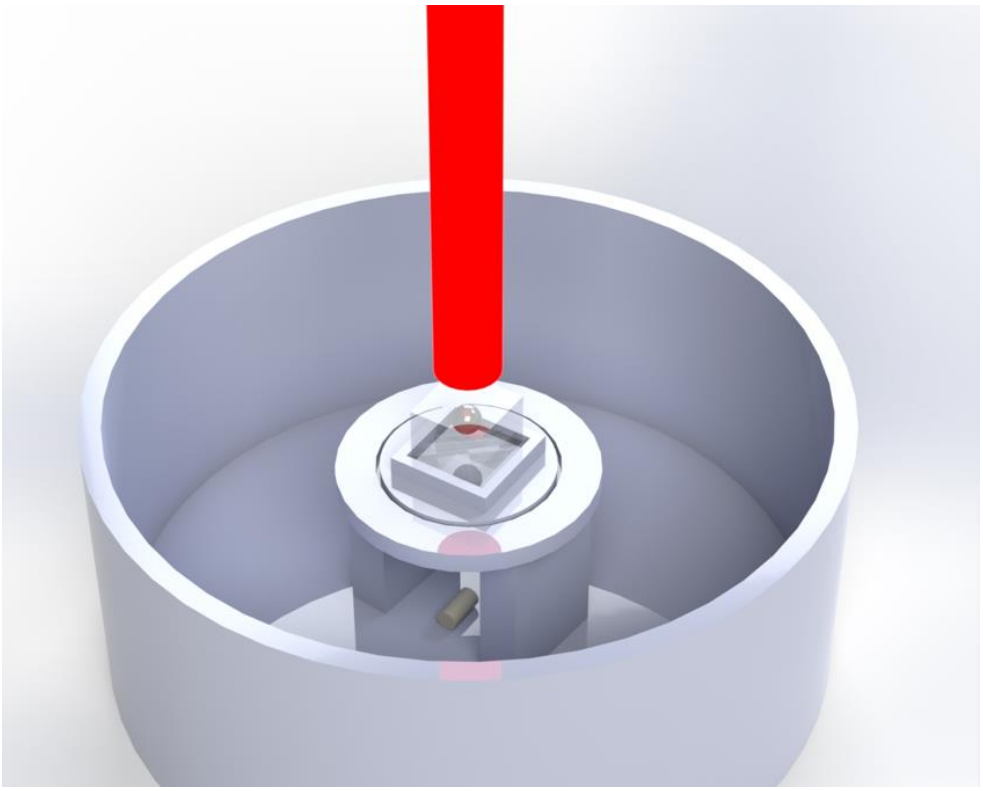

Figure 5: Illustrative model of laser delivery to phantoms. Phantoms are staged on the center platform, while a stir bar underneath slowly circulates water to maintain a constant temperature. (Model Credit: Aidan Canning)

Phantom staging and alignment were done using a simple laser viewing card placed on the top layer of each phantom in a dark environment. For each phantom, it was ensured that the thin top layer of the phantom (described previously) was above the water level and exposed to air, mimicking animal and patient surface skin exposure to air. Importantly, a similar alignment procedure is performed prior to animal laser treatments. This step is vital to ensuring energy deposition to the desired "treatment" volume (phantom or animal) during laser delivery, as well as minimizing healthy tissue laser exposure. Once centering of the phantom under the laser beam was confirmed,

thermocouples were placed into their desired locations in the phantoms (outlined in more detail in the next section), followed by a waiting period for the phantom-water system to reach thermal equilibrium, confirmed by thermocouple readings.

Once phantom-laser alignment, thermocouple placement and thermal equilibrium were confirmed, the phantoms were ready for laser delivery. For the presented phantom work, two laser delivery techniques were employed: Continuous (at various power densities) and Cyclic. Continuous delivery corresponds to an uninterrupted, constant power density beam delivery. Cyclic delivery corresponds to a constant power density beam delivery for a fixed amount of time, then the beam is turned off for a fixed amount of time, then turned back on, etc. Continuous delivery was chosen simply to replicate standard SYMPHONY treatment and cyclic delivery was chosen to demonstrate how high local temperatures are maintained due to GNS heating even when the laser beam is off (this is a considerable motivation for potential pulsed laser delivery schemes and surface skin dose sparing considerations).

Each phantom underwent continuous delivery, where 30 seconds of thermocouple temperature data was collected without the beam to establish the initial temperature at each thermocouple position, followed by 10 minutes of continuous beam delivery at a 0.5 W/cm^2 power density. Then, both the homogeneous and heterogeneous 0.5 nM phantoms were exposed to continuous delivery at 0.25 and 0.75 W/cm^2 to investigate the effects of power density scaling on temperature. Finally, both 0.5 nM

phantoms were exposed to cyclic beam delivery, where the beam is turned on for 1 minute then off for two minutes.

The completion of this phantom work resulted in a large volume of temperature data, consisting of 18 total phantoms (1 blank, 8 homogeneous, 8 heterogeneous and 1 star shape) and a multitude of thermocouples placed in each phantom during beam delivery (summarized in the Results section). Such an extensive characterization of the GNS-mediated photothermal effect in phantoms had not been previously demonstrated and represents a significant contribution to the development of the SYMPHONY treatment. Additionally, the large library of phantom temperature data provides a direct method for validation of this work's proposed simulation method. The ability to create predictive photothermal simulations that accurately recreates phantom data will motivate the application of the simulation method to *in vivo* animal studies and beyond.

2.4.4 Thermal Dosimetry

The chosen method for thermal dosimetry in this work is implanted thermocouple. While there are considerable disadvantages to this method, most importantly the lack of complete volumetric temperature data, it is a simple, cost-effective method for collecting temperature data over time, with high precision.

For the homogeneous phantom experiments, a thermocouple array was inserted (see picture below), which collects data across multiple depths. For the heterogeneous

phantoms, multiple thermocouples were inserted at various spatial locations; in the top "skin" layer, within the GNS spherical volume and in the normal agarose gel.

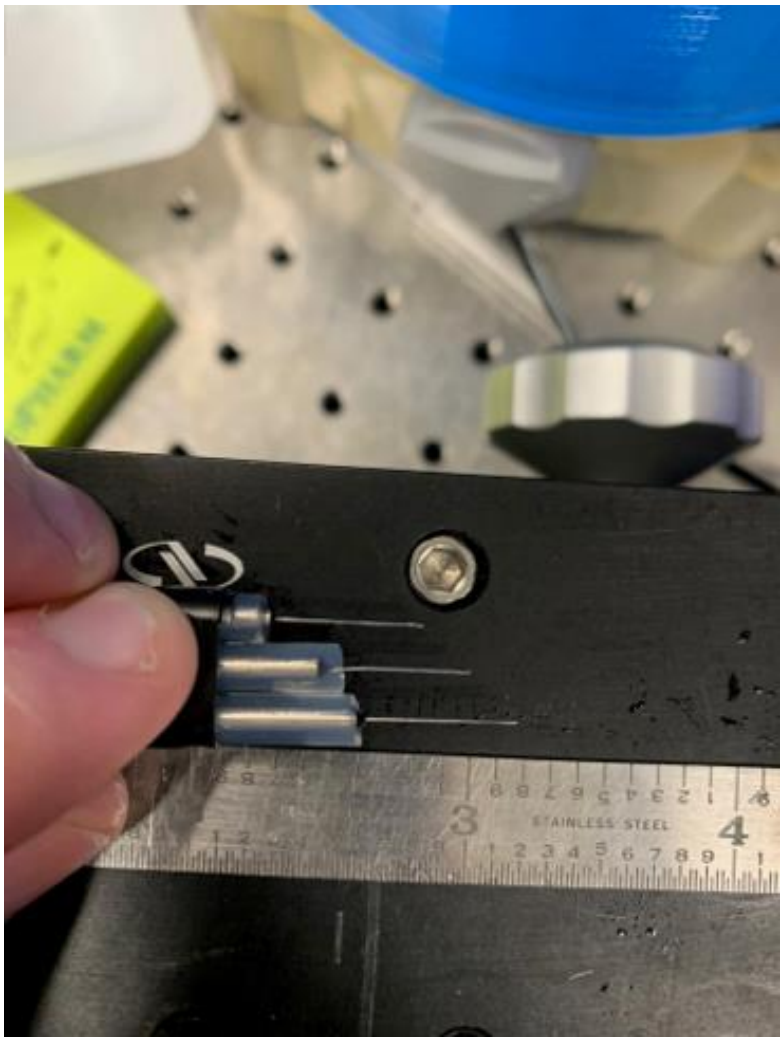

Figure 6: Thermocouple array placed in phantoms for thermal dosimetry

Future experiments, both *in vitro* and *in vivo,* will include this "invasive" thermal dosimetry as well as "non-invasive" temperature imaging techniques (talked about more in the Discussion section).

3. Results

3.1 Material Characterization

For this work, only initial optical absorbance characterization of GNS was performed. However, a complete characterization of the thermal and dielectric properties as well will be required for the use of GNS in human trials.

3.1.1 Optical Absorption

Shown below is the absorbance curve generated using the absorbance value of 0.45267 for agarose gel uniformly mixed with 0.5 nM GNS. This linear curve was generated using this value and Equation 1.

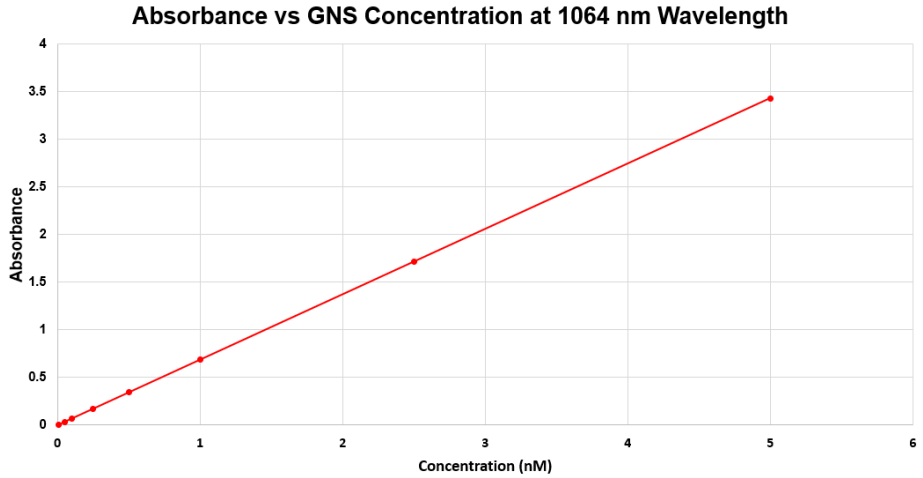

Figure 7: Optical absorbance versus GNS concentration

These optical absorbance values, along with scattering coefficients taken from literature serve as the basis for the selected optical properties that are simulated.

3.2 In Vitro Photothermal Characterization/Modeling

At the time of completion for this thesis, final modifications to the COMSOL thermal models were being made, so the results of these simulations are not presented here. They will however be used to validate the simulation method and compare to temperature acquired during the presented experiments. For brevity, homogeneous temperature curves acquired during experiment are presented with their corresponding optical simulations for analysis.

3.2.1 Homogeneous Phantoms

The experimental setup of the homogeneous phantoms was replicated in MCMatlab, with corresponding optical properties of the materials present in the system. A collimated, top-hat beam of radius 0.8 cm was simulated, replicating the laser delivery performed during the experiments. Simulations were performed for 10 minutes, typically simulating over 1 million photons. Presented next are results from the homogeneous phantom heating experiments and their optical simulations.

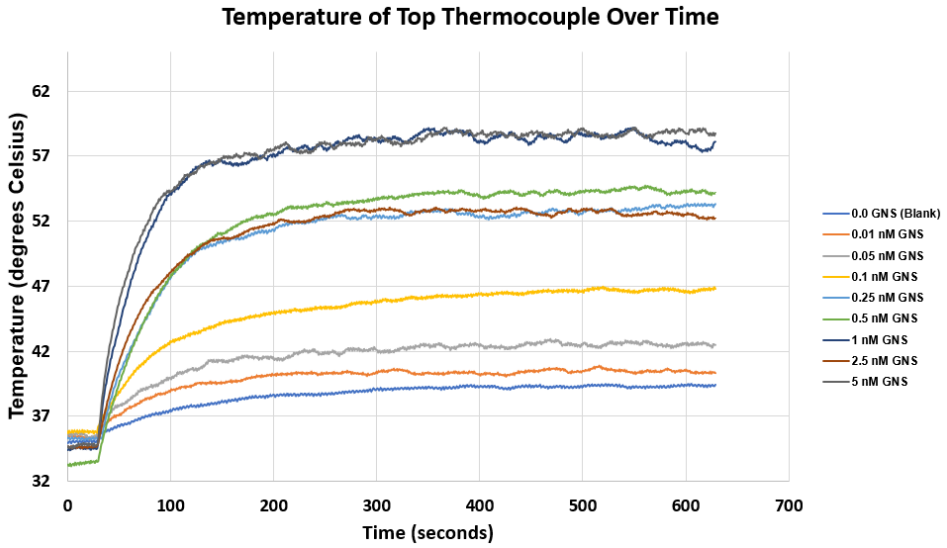

Figure 8: Temperature of the top thermocouple over time during 10 minutes of 0.5 W/cm^2 laser delivery

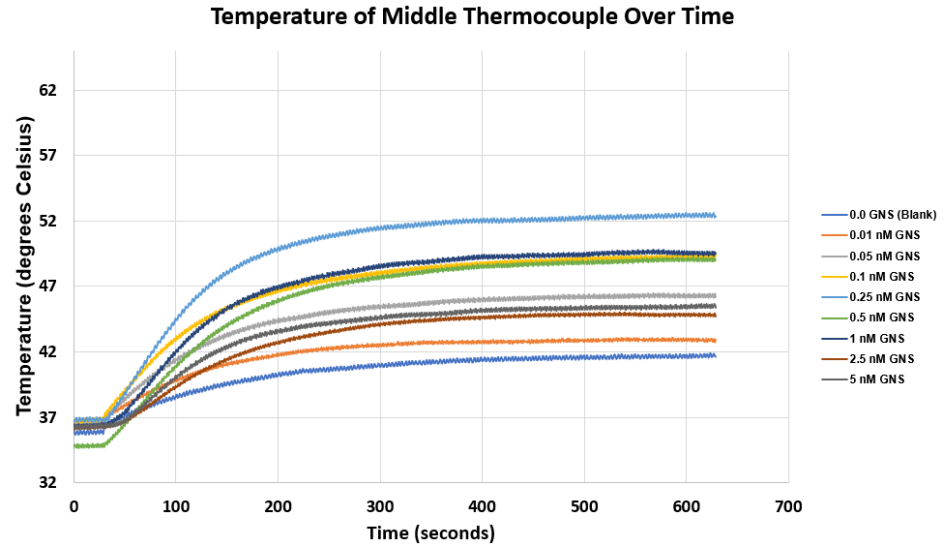

Figure 9: Temperature of the middle thermocouple over time during 10 minutes of 0.5 W/cm^2 laser delivery

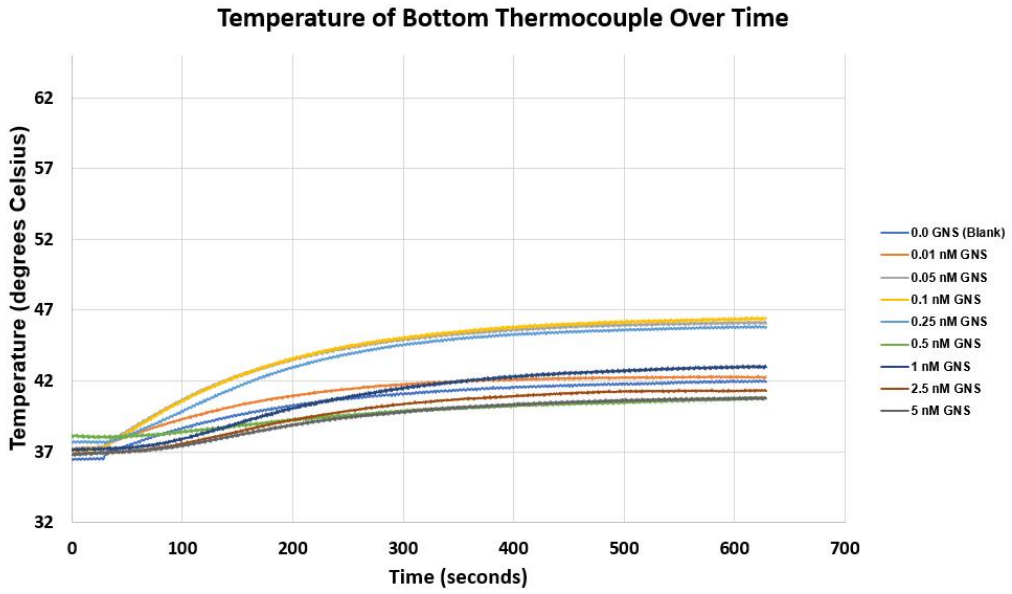

Figure 10: Temperature of the bottom thermocouple over time during 10 minutes of 0.5 W/cm^2 laser delivery

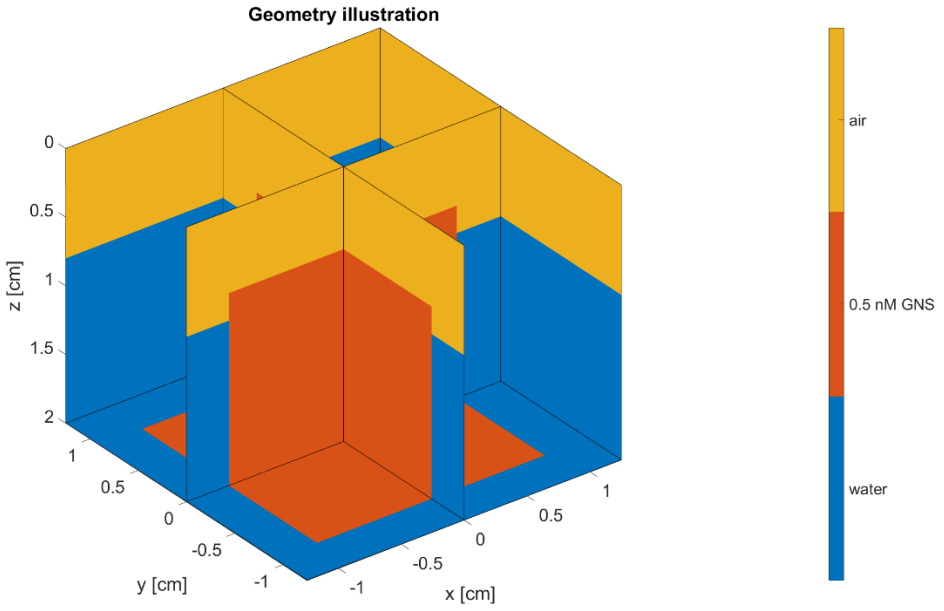

Figure 11: Example MCMatlab homogeneous phantom optical geometry for 0.5 nM GNS

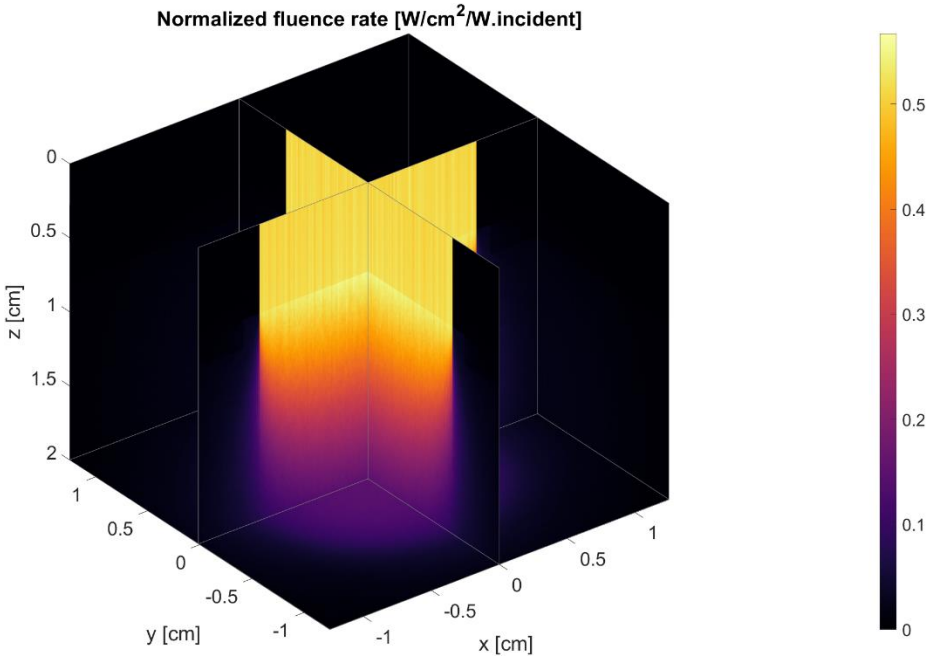

Figure 12: Example resulting fluence distribution for 0.5 nM GNS homogeneous phantom

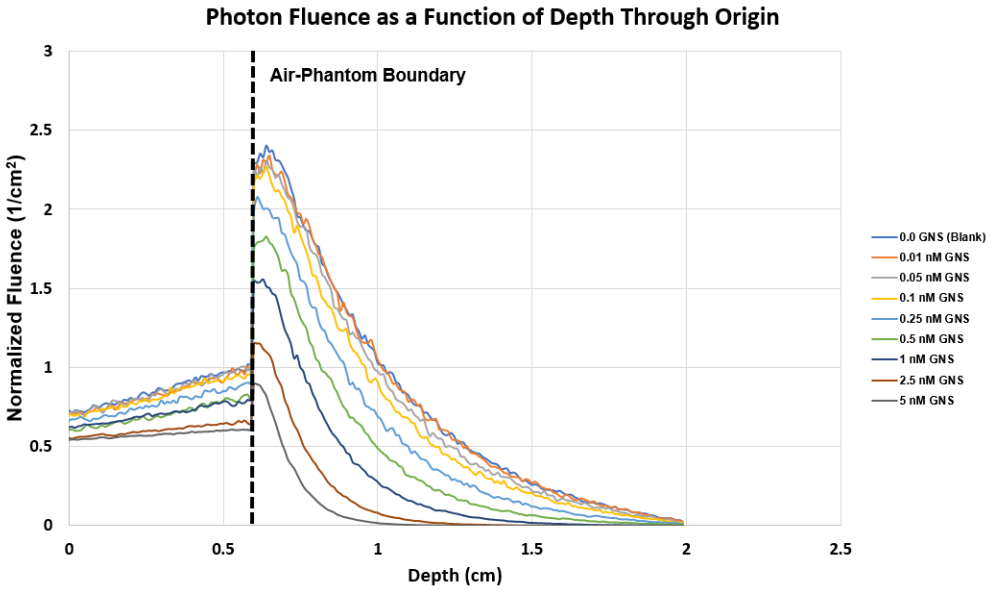

Figure 13: Line profile of fluence through the origin for each concentration

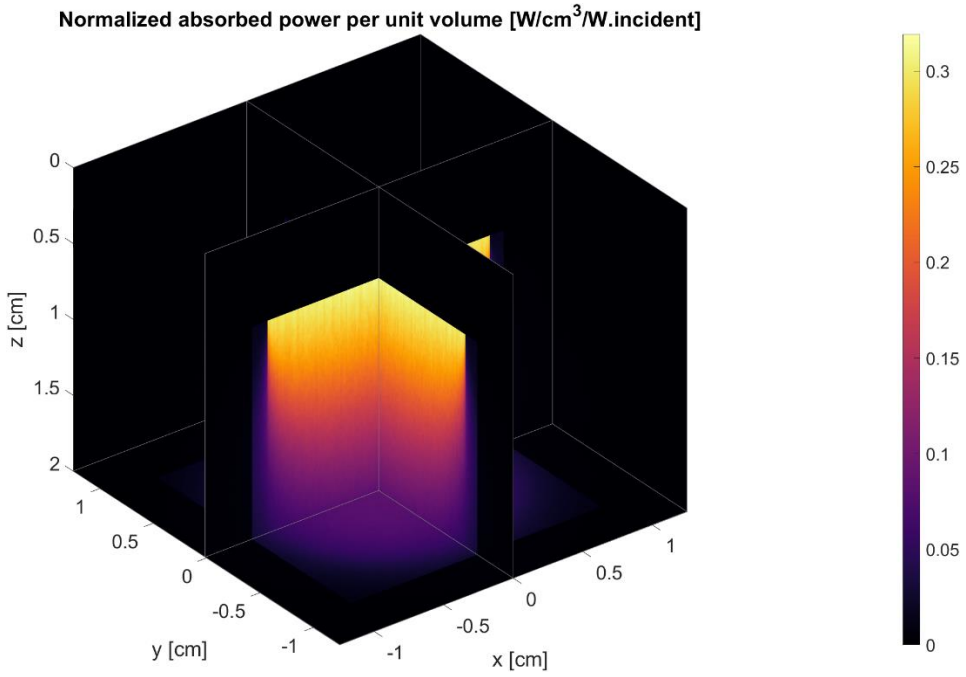

Figure 14: Example resulting absorption for 0.5 nM GNS homogeneous phantom

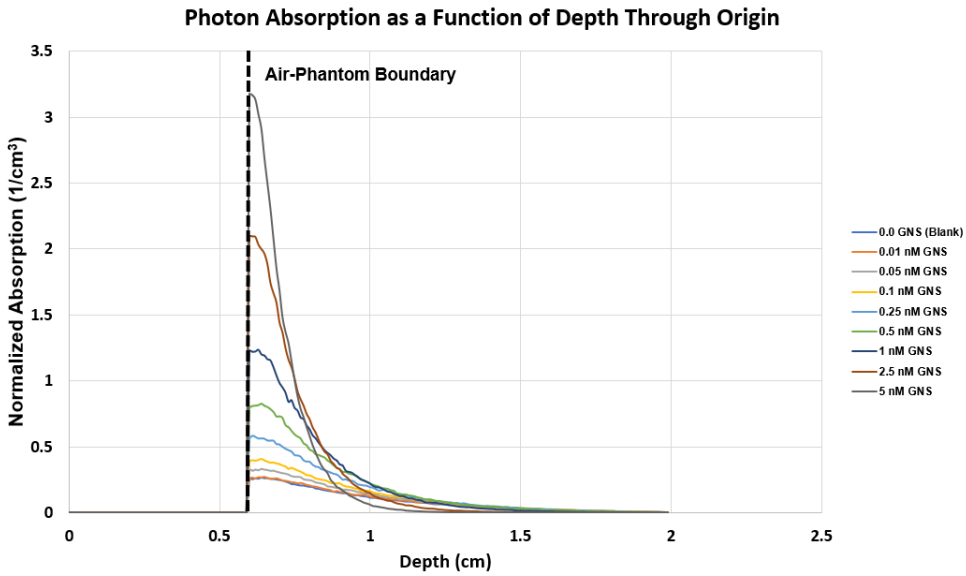

Figure 15: Line profile of absorption through the origin for each concentration

3.2.1 Heterogeneous Phantoms

Like above, the heterogeneous optical geometry was recreated in MCMatlab with the same beam and optical parameters. Optical simulations were performed for the same time across the GNS concentration range. The results of the optical simulations for the heterogeneous phantoms are not presented here for brevity.

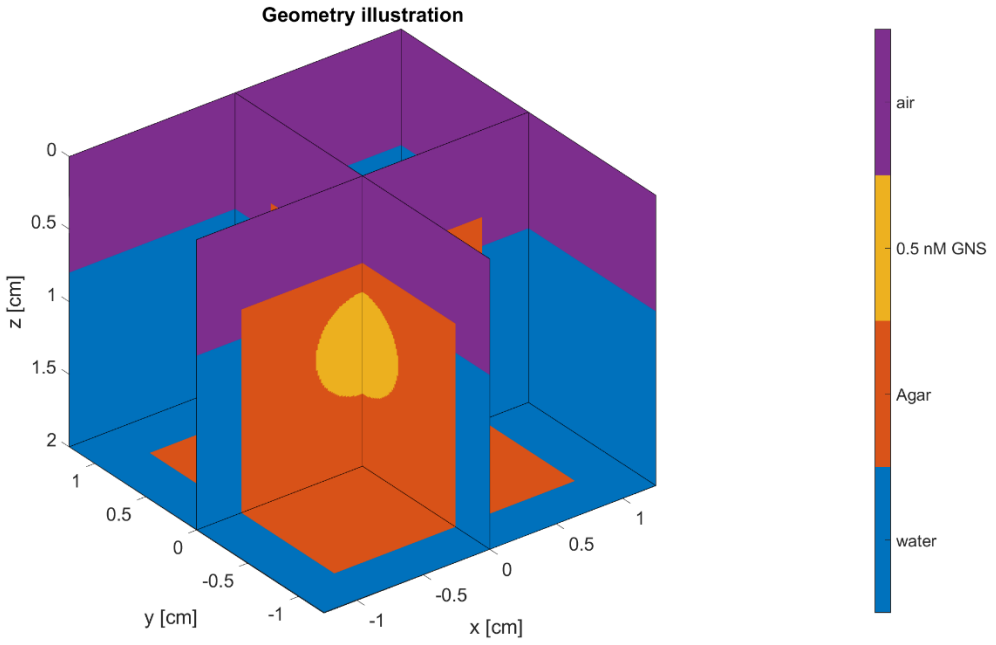

Figure 16: Example MCMatlab heterogeneous phantom optical geometry for 0.5 nM GNS

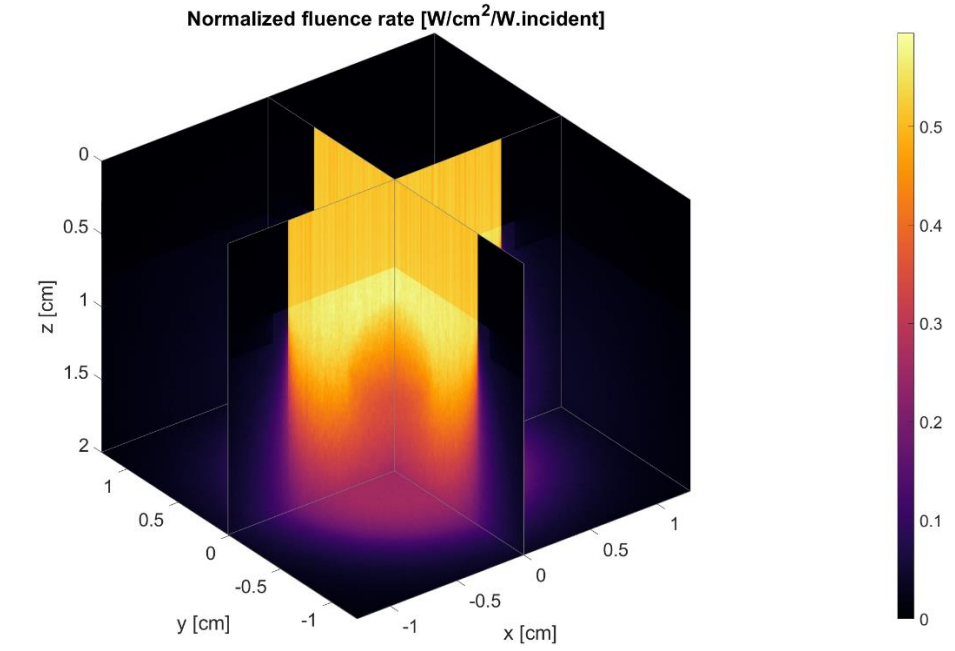

Figure 17: Example resulting fluence distribution for 0.5 nM GNS heterogeneous phantom

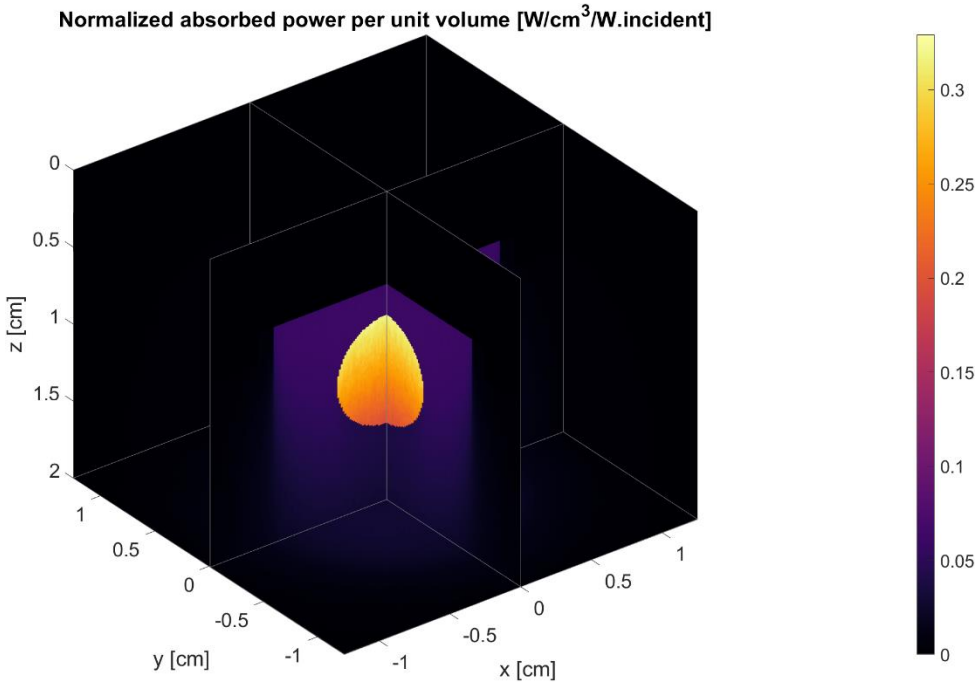

Figure 18: Example resulting absorption for 0.5 nM GNS heterogeneous phantom

4. Conclusion

This work presented a simulation method that can be further adapted into a photothermal treatment planning workflow for SYMPHONY. Further investigation and quantification of the GNS-mediate photothermal effect will be crucial in the translation of SYMPHONY to human trials for the treatment of metastatic disease.

4.1 Presented Data

In the presented phantom heating data, many insightful trends are available to analyze the photothermal effect when GNS are present. Firstly, the initial slope of temperature increase across GNS concentrations in Figure 8 highlights the stark increase in optical absorption as the concentration of GNS increases. As a result, for higher concentrations, the heating of the bottom thermocouple is lowered. As an extreme case (as this concentration has not been seen in tissue in biodistribution studies), 5 nM GNS exhibits the highest optical absorption at the phantom surface. This led to temperature increases up to nearly 60 degrees Celsius. However, the temperature of the bottom thermocouple in the phantom is the lowest for 5 nM. This is due to optical absorption being dominated at the phantom surface, not allowing significant penetration of photons towards the bottom of the phantom. In the context of animal and human treatments, this phenomenon would lead to increased thermal skin dose, and reduced tumor temperature, which is not therapeutically ideal.

Such phenomenon exhibited in phantom heating studies can be used to inform *in vivo* treatment planning and delivery decision making, with the results of this work highlighting their importance for biomedical optics in cancer care.

4.2 Study Limitations

Inherent to Monte Carlo simulations, statistical noise was present in the simulation results. Increasing the simulation duration, and thus the number of simulated photons, will reduce statistical noise in the optical absorptions results. This will in turn lead to more accurate heating models.

As identified previously thermocouple dosimetry, while straightforward, is not a complete method for photothermal dosimetry. Described next, temperature imaging techniques will be required for future iterations of SYMPHONY treatment.

While phantom studies can prove vital for demonstrating key optical phenomena, many biological effects and processes cannot be replicated in a phantom. This becomes particularly evident in pre-clinical cancer therapy research, and future studies for SYMPHONY development will need extensive phantom and animal work, in tandem.

4.3 Future Work

In this work, a photothermal simulation technique was introduced as a potential treatment planning workflow for SYMPHONY treatment. Characterization of the GNS mediated photothermal effect was performed through agarose-GNS gel phantom

heating studies, with accompanying photothermal simulations used for validation of the method.

Outlined next are potential directions for future studies following this work. Continued advances and developments in SYMPHONY's photothermal therapy arm are vital to establishing SYMPHONY as a clinically translatable and viable treatment option for metastatic bladder cancer.

4.3.1 Continued Phantom Heating Experiments

Both the versatility and utility of tissue-mimicking phantom studies in optical applications to cancer therapy have established them as a powerful tool to demonstrate laser-tissue interaction phenomenon, as shown in this work's experiments.

Planned in upcoming experiments are more sophisticated phantom fabrications that more accurately replicate the optical environment present in biological tissue implanted with GNS. Specifically, replicating the homogeneous and heterogeneous structures presented in this work with the addition of a highly scattering material. Intralipid (a lipid emulsion) will be introduced during phantom fabrication, more accurately emulating the scattering properties of tissue compared to agarose alone, which is essentially water equivalent.

Subsequent heating studies using these phantoms and their corresponding photothermal simulations will provide additional time-resolved temperature data to further validate the simulation technique and characterize the GNS photothermal effect.

4.3.2 Animal Laser Power Density Study and Simulation

While phantom studies provide valuable information on the GNS photothermal effect, the overall goal for the extension of this work is to develop an image-based treatment planning component of SYMPHONY. This workflow must be experimentally validated in both phantom and animal studies, and eventually validated in human trials.

Currently, animal laser heating comparison studies are being planned to investigate the tumor heating effects at various laser power densities, with temperature data collected by implanted thermocouple. The *in vivo* temperature data will be compared to simulation data generated from 3D models developed from segmentation of GNS PET/CT image sets. Validation of the accuracy of the treatment planning method in an *in vivo* setting will provide strong motivation for SYMPHONY's translation to humans.

4.3.3 Incorporation of Non-Invasive Temperature Imaging Techniques

Future development of SYMPHONY's photothermal arm will include advancements in temperature feedbacks systems and thermal dosimetry. Our group has extensive experience in magnetic resonance thermal imaging and microwave radiometry, with each being developed for standard incorporation into the SYMPHONY treatment workflow. The use of these techniques will allow for complete acquisition of volumetric temperature data over time, with real-time temperature feedback during laser delivery.

An additional method for temperature imaging used during SYMPHONY treatment is an infrared camera. While this imaging technique does not provide depth resolved temperature information, it is used as an effective method for skin temperature monitoring during treatment.

In both phantom and animal laser heating studies, incorporation of the above imaging techniques will offer invaluable temperature data that demonstrates the GNS-mediated photothermal effect. Additionally, acquired temperature data will also serve as a way of retrospectively validating photothermal simulations. Use of a fully standardized laser delivery system, including a temperature imaging feedback system, is a vital aspect of SYMPHONY that should be developed in upcoming studies.

References

1) If you have bladder cancer. American Cancer Society. (n.d.). Retrieved February 21, 2022, from https://www.cancer.org/cancer/bladder-cancer/if-you-have-bladder-cancer.html

2) Antoni, S., Ferlay, J., Soerjomataram, I., Znaor, A., Jemal, A., & Bray, F. (2017). Bladder cancer incidence and mortality: A global overview and recent trends. *European Urology*, *71*(1), 96–108. https://doi.org/10.1016/j.eururo.2016.06.010

3) von der Maase, H., Sengelov, L., Roberts, J. T., Ricci, S., Dogliotti, L., Oliver, T., Moore, M. J., Zimmermann, A., & Arning, M. (2005). Long-term survival results of a randomized trial comparing gemcitabine plus cisplatin, with methotrexate, vinblastine, doxorubicin, plus cisplatin in patients with bladder cancer. *Journal of Clinical Oncology*, *23*(21), 4602–4608. https://doi.org/10.1200/jco.2005.07.757

4) Stenehjem, D., Tran, D., Nkrumah, M., & Gupta, S. (2018). PD1/PDL1 inhibitors for the treatment of advanced urothelial bladder cancer. *OncoTargets and Therapy*, *Volume 11*, 5973–5989. https://doi.org/10.2147/ott.s135157

5) Pirzada, M., Ghauri, R., Ahmed, M., Shah, M., Nasir, I. ul, Siddiqui, J., Ahmed, I., & Mir, K. (2017). Outcomes of BCG induction in high-risk non-muscle-invasive bladder cancer patients (NMIBC): A retrospective cohort study. *Cureus*. https://doi.org/10.7759/cureus.957

6) Inman, B. A., Sebo, T. J., Frigola, X., Dong, H., Bergstralh, E. J., Frank, I., Fradet, Y., Lacombe, L., & Kwon, E. D. (2007). PD-L1 (B7-H1) expression by urothelial carcinoma of the bladder and BCG-induced granulomata. *Cancer*, *109*(8), 1499–1505. https://doi.org/10.1002/cncr.22588

7) Lee, H., Lee, S., & Heo, Y.-S. (2019). Molecular interactions of antibody drugs targeting PD-1, PD-L1, and CTLA-4 in immuno-oncology. *Molecules*, *24*(6), 1190. https://doi.org/10.3390/molecules24061190

8) Balar, A. V., Castellano, D., O'Donnell, P. H., Grivas, P., Vuky, J., Powles, T., Plimack, E. R., Hahn, N. M., de Wit, R., Pang, L., Savage, M. J., Perini, R. F., Keefe, S. M., Bajorin, D., & Bellmunt, J. (2017). First-line pembrolizumab in cisplatin-ineligible patients with locally advanced and unresectable or metastatic

urothelial cancer (Keynote-052): A Multicentre, single-arm, phase 2 study. *The Lancet Oncology*, *18*(11), 1483–1492. https://doi.org/10.1016/s1470-2045(17)30616-2

9) Repasky, E. A., Evans, S. S., & Dewhirst, M. W. (2013). Temperature matters! and why it should matter to tumor immunologists. *Cancer Immunology Research*, *1*(4), 210–216. https://doi.org/10.1158/2326-6066.cir-13-0118

10) Liu, X., Shan, G., Yu, J., Yang, W., Ren, Z., Wang, X., Xie, X., Chen, H.-jiuan, & Chen, X. (2017). Laser heating of metallic nanoparticles for photothermal ablation applications. *AIP Advances*, *7*(2), 025308. https://doi.org/10.1063/1.4977554

11) Yuan, H., Khoury, C. G., Hwang, H., Wilson, C. M., Grant, G. A., & Vo-Dinh, T. (2012). Gold Nanostars: Surfactant-free synthesis, 3D modelling, and two-photon photoluminescence imaging. *Nanotechnology*, *23*(7), 075102. https://doi.org/10.1088/0957-4484/23/7/075102

12) Kong, G., Braun, R. D., & Dewhirst, M. W. (2000). Hyperthermia enables tumor-specific nanoparticle delivery: effect of particle size. *Cancer research*, *60*(16), 4440–4445.

13) Liu, Y., Maccarini, P., Palmer, G. M., Etienne, W., Zhao, Y., Lee, C.-T., Ma, X., Inman, B. A., & Vo-Dinh, T. (2017). Synergistic immuno photothermal nanotherapy (symphony) for the treatment of unresectable and metastatic cancers. *Scientific Reports*, *7*(1). https://doi.org/10.1038/s41598-017-09116-1

14) Liu, Y., Ashton, J. R., Moding, E. J., Yuan, H., Register, J. K., Fales, A. M., Choi, J., Whitley, M. J., Zhao, X., Qi, Y., Ma, Y., Vaidyanathan, G., Zalutsky, M. R., Kirsch, D. G., Badea, C. T., & Vo-Dinh, T. (2015). A plasmonic gold Nanostar theranostic probe for in vivo tumor imaging and photothermal therapy. *Theranostics*, *5*(9), 946–960. https://doi.org/10.7150/thno.11974

15) Amendola, V., & Meneghetti, M. (2009). Size evaluation of gold nanoparticles by UV−Vis Spectroscopy. *The Journal of Physical Chemistry C*, *113*(11), 4277–4285. https://doi.org/10.1021/jp8082425

16) Libretexts. (2021, March 21). *4.4: UV-visible spectroscopy*. Chemistry LibreTexts. Retrieved February 18, 2022, from https://chem.libretexts.org/Bookshelves/Analytical_Chemistry/Physical_Methods

_in_Chemistry_and_Nano_Science_(Barron)/04%3A_Chemical_Speciation/4.04%3A_UV-Visible_Spectroscopy#:~:text=For%20a%20single%20wavelength%2C%20A,of%20the%20solution%20(M)

17) Wang, L., Jacques, S. L., & Zheng, L. (1995). MCML—Monte Carlo Modeling of light transport in multi-layered tissues. *Computer Methods and Programs in Biomedicine*, *47*(2), 131–146. https://doi.org/10.1016/0169-2607(95)01640-f

18) Marti, D., Aasbjerg, R. N., Andersen, P. E., & Hansen, A. K. (2018). MCmatlab: An open-source, user-friendly, MATLAB-integrated three-dimensional Monte Carlo light transport solver with heat diffusion and tissue damage. *Journal of Biomedical Optics*, *23*(12), 1. https://doi.org/10.1117/1.jbo.23.12.121622